Projected and slice emittance measurements using multi-quadrupole scan and streak readout at PITZ

R. Spesyvtsev, DESY, Zeuthen site

September 14, 2009

1 Introduction

The Photo Injector Test Facility at DESY, Zeuthen site (PITZ), has been built to develop and characterize photo injectors with a high quality electron beam. One of the main characteristics of the beam is its normalized emittance. Development of injectors is targeted towards producing beams with low normalized emittance, thus high resolution emittance measurement setups are required. One of the current goals of the facility is to obtain a low projected emittance in the order of 0.9 mm mrad for 1 nC bunch charge. During the charge emission from the photocathode and an early stage electron bunch acceleration space charge forces contribute significantly to the development of short electron bunches. The influence of the space charge on the emittance varies within the electron bunch. Therefore emittance is changing within the electron bunch. While the middle part of the bunch has low emittance, the head and tail of the bunch contribute to the projected emittance growth. The slice emittance can be as low as 0.6 mm mrad in the middle of the bunch. Thus, the resolution requirements to the slice emittance measurement setup are even higher than to the projected emittance measurement setup.

Currently, the slit scan technique is being used to measure the normalized projected emittance at PITZ. The simulation results cause much interest in developing and implementing a slice emittance measurement technique at PITZ. Two methods are under development for the slice emittance measurements: quadrupole scan (or slit scan) technique with an energy chirped beam and quadrupole scan technique with a streak readout. In addition, the installation of a transverse deflecting cavity (TDC) is planned in the future for time resolved measurements of the bunch properties including the slice emittance. In this report the systematic error of the quadrupole scan technique with a streak readout is presented. The advantage of a multiquadrupole scheme is shown which has the possibility to improve a quadrupole scan technique for the emittance measurements. A multiquadrupole structure can be used to lower the resolution requirements by controlling the beam dimensions at the screen for both the projected and the slice emittance measurements.

2 Theoretical aspects

2.1 Basic concept

The emittance measurement technique, which is based on the quadrupole scan, uses a linear matrix formalism [1]. In the ideal case, there are no correlations between the transverse directions X and Y and therefore beam properties in the transverse plane can be described for each direction separately using the 2D beam matrix:

$$\sigma = \begin{pmatrix} \sigma_{11} & \sigma_{12} \\ \sigma_{21} & \sigma_{22} \end{pmatrix} = \begin{pmatrix} < x^2 > & < xx' > \\ < xx' > & < x'^2 > \end{pmatrix}, \tag{1}$$

where $< x^2 >$ and $< x'^2 >$ are the second order moments of the coordinate and the angular distributions and $< xx' >$ is the correlation between them. Furthermore, $\sqrt{< x^2 >}$ is the beam rms size and $\sqrt{< x'^2 >}$ is the beam rms divergence. Using this definition, the rms emittance can be calculated as $\varepsilon_{rms} = \sqrt{det(\sigma)}$ and the normalized emittance:

$$\varepsilon_n = \gamma\beta\sqrt{det(\sigma)}, \tag{2}$$

where γ and β are the energy and velocity factors, respectively.

In this formalism, beam propagation through the beam line is a transformation of a beam matrix from one beam line element to another [2] [3]. For the quadrupole scan, three types of transformation matrices are used:

$$\begin{aligned} &Drift\ space: && R_d = \begin{pmatrix} 1 & l \\ 0 & 1 \end{pmatrix}, where\ l\ is\ the\ drift\ length \\ &Focusing\ quadrupole: && R_f = \begin{pmatrix} \cos(\phi) & \frac{1}{\sqrt{k}}\sin\phi \\ -\sqrt{k}\sin\phi & \cos\phi, \end{pmatrix} \\ &Defocusing\ quadrupole: && R_{df} = \begin{pmatrix} \cosh(\phi) & \frac{1}{\sqrt{k}}\sinh\phi \\ \sqrt{k}\sinh\phi & \cosh\phi, \end{pmatrix} \end{aligned} \tag{3}$$

where k is the quadrupole strength, $\phi = l_{eff}\sqrt{k}$, l_{eff} is the effective length of the quadrupole magnet. The quadrupole strength can be derived through the quadrupole gradient g and the beam momentum p [3]:

$$k[m^{-2}] = 0.2998\frac{g[T/m]}{p[GeV/c]} \tag{4}$$

It is important to notice that the description above does not include any interaction between the particles in the bunch, thus space charge effects are missing in this theory. There are no analytical solutions for the space charge contribution, but it is possible to solve envelope equations with space charge numerically for some simplified geometries [2] [4]. In practise, the focal length f of the quadrupole magnet is usually much larger than its effective length:

$$f = \frac{1}{k \cdot l_{eff}} \gg l_{eff} \tag{5}$$

Therefore, the transformation matrices for the quadrupole magnet could be simplified to:

$$R_f = \begin{pmatrix} 1 & 0 \\ -\frac{1}{f} & 1 \end{pmatrix}, \quad R_{df} = \begin{pmatrix} 1 & 0 \\ \frac{1}{f} & 1 \end{pmatrix} \tag{6}$$

The beam matrix propagation through any of the beam line elements can be described in the following way:

$$\sigma = RaR^T, \tag{7}$$

where a is the initial beam matrix and σ is the beam matrix after the propagation of the beam through the element with the transformation matrix R. In cases where there is more than one element, the total transformation matrix will be a multiplication of each subsequent part: $R = ...R_3R_2R_1$. The order of the multiplication is very important: the beam matrix of the first beam line element on the way of the beam should be placed to the right.

For clarity, the following definitions will be used during the derivations below: X and Y directions create a transverse plane, the X direction will always be used as the direction of measurement. All quadrupole matrices are focusing in the X direction when $k > 0$ and therefore defocusing in the Y direction, when $k > 0$.

2.2 Data fitting procedure

The main goal of the quadrupole scan experiment is to determine the beam matrix a in front of the quadrupole. During the experiment, the beam propagates through the system of quadrupole magnets and drift spaces with known transformation matrices R and the beam size at the screen location, $\sqrt{\sigma_{11}}$, is measured. Using the first matrix element in Eq. (7), a linear equation can be obtained:

$$\sigma_{11} = R_{11}^2 a_{11} + 2R_{11}R_{12}a_{12} + R_{12}^2 a_{22} = F(k, a_{11}, a_{12}, a_{22}) \tag{8}$$

Changing the transformation matrix R by altering the quadrupole strength, a system of independent equations may be obtained. The model which describes the behavior of σ_{11} is never perfect due to the complicated space charge forces and the longitudinal momentum distribution. Besides this, the measured values of σ_{11}^i always have some uncertainty. Therefore, the standard least-squares method was used to determine a_{11}, a_{12} and a_{22} parameters, where the function to be minimized is:

$$\chi^2 = \sum_{i=1}^{n} \left(\frac{\sigma_{11}^i - F(k_i, a_{11}, a_{12}, a_{22})}{\delta\sigma_{11}^i} \right)^2 \tag{9}$$

where σ_{11}^i is the measured second moment of the beam distribution, with its standard deviation ($\delta\sigma_{11}^i$) at a corresponding quadrupole strength k_i. Using a minimization tool from any scientific software (Mathematica, MINUIT, MATLAB, etc.) the beam matrix a can be found and the normalized beam emittance can be easily calculated (Eq. (2)).

2.3 Error estimation

It is important to know the uncertainty of the measurements in order to validate the obtained experimental results. There are two types of measurement uncertainty: statistical and systematic. This section considers only statistical uncertainty estimation. Estimation of the systematic uncertainty is more complicated. Main types of systematic uncertainty and their estimation procedure are described in Section 4.

The main assumption in this section is that all errors are normally distributed. For each measurement point a series $\{x_n\}$ of n independent measurements is taken, afterwards the mean value $< x >$ and the standard deviation $\sqrt{< x^2 >}$ can be determined as:

$$< x >= \sum_{i=1}^{n} \frac{x_i}{n}, \quad \sqrt{< x^2 >} = \sum_{i=1}^{n} \frac{(< x > -x_i)^2}{n-1} \tag{10}$$

Mean value $< x >$ represents a result of the measurement and standard deviation represents an error of this measurement. The meaning of this error is that with a probability of 68.3% any single measurement x_i will be inside of the interval $< x > \pm\sqrt{< x^2 >}$. Applying minimization procedure of Eq. (9) to n independent sets of data, the series $\{\epsilon_n\}$ of n independent emittance values can be obtained and a mean value and a standard deviation can be calculated in the same way (10).

2.4 Single quadrupole scan

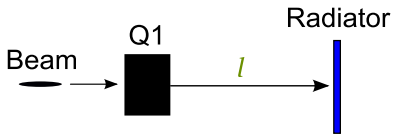

Figure 1: Single quadrupole scan scheme.

The single quadrupole scan system consists of a quadrupole magnet and a drift space (Fig. 1). The transformation matrix of this system for the X direction can be obtained from Eqs. (3) (6) $R = R_d R_f$:

$$R = \begin{pmatrix} 1 - \frac{l}{f} & l \\ -\frac{1}{f} & 1 \end{pmatrix} \tag{11}$$

Thus Eq. (8) expands to

$$\sigma_{11} = \left(1 - \frac{l}{f}\right)^2 a_{11} + 2\left(1 - \frac{l}{f}\right) l a_{12} + l^2 a_{22} \tag{12}$$

σ_{11} is measured at the radiator location for the different values of $\frac{1}{f}$ which is varied by changing the quadrupole current. It is clear that the function $\sigma_{11}(\frac{1}{f})$ is a second order polynomial. Solving equation

$$\frac{d\sigma_{11}}{d(\frac{1}{f})} = 0 \tag{13}$$

it is easy to find the minimum of σ_{11} and its location:

$$\sigma_{11min} = \frac{\varepsilon_{rms}^2 l^2}{a_{11}} = \frac{\varepsilon_n^2 l^2}{\gamma^2 \beta^2 a_{11}} \tag{14}$$

$$\frac{l}{f} = 1 + \frac{a_{12}}{a_{11}} l, \tag{15}$$

Eq. (14) defines the limitation for the emittances that the setup can measure. From one side it is limited by the radiator dimensions and from the other, by the resolution of the beam size measurement system. The normalized emittance in (14) needs to be measured. All other parameters can be optimized for the measurement procedure. Since the development of the injectors is tending towards lower emittances, the beam size at the minimum location decreases and the resolution of the measurement setup plays an important role.

2.5 Double quadrupole scan

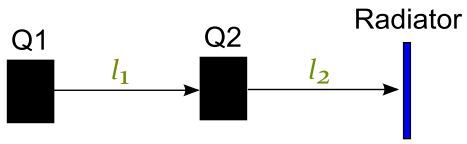

Figure 2: Double quadrupole scan scheme.

The double quadrupole system includes two quadrupoles with their focal lengths f_1 and f_2 and two drift spaces l_1 and l_2 (Fig. 2). Although a transformation matrix of a double quadrupole system is more complicated than for a single quadrupole system $R = R_{d2}R_{f2}R_{d1}R_{f1}$, it gives more flexibility to choose the range of σ_{11}^X for the measurements. Furthermore, it is useful to optimize Yrms beam size $\sqrt{\sigma_{11}^Y}$ as well, which is possible since there are more parameters to control. Only two terms of the matrix R are required for Eq. (8):

$$R_{11}^X = \left(1 - \frac{l_2}{f_2}\right)\left(1 - \frac{l_1}{f_1}\right) - \frac{l_2}{f_1}, \quad R_{12}^X = \left(1 - \frac{l_2}{f_2}\right) l_1 + l_2 \tag{16}$$

$$R_{11}^Y = \left(1 + \frac{l_2}{f_2}\right)\left(1 + \frac{l_1}{f_1}\right) + \frac{l_2}{f_1}, \quad R_{12}^Y = \left(1 + \frac{l_2}{f_2}\right) l_1 + l_2 \tag{17}$$

The difference between X and Y transformation matrices for a quadrupole magnet is the sign of the quadrupole gradient (focal length). Applying the extremum condition to $\sigma_{11}^X(\frac{1}{f_1}\frac{1}{f_2})$:

$$\frac{\partial \sigma_{11}^X}{\partial(\frac{1}{f_1})} = 0 \tag{18}$$

and using Eqs. (8) (16), the location of the σ_{11}^X minimum can now be found for any arbitrary value of f_2. Eq. (18) has two solutions:

$$\sigma^X_{11min} = \frac{\varepsilon^2_{rms} l_1^2}{a^X_{11}} \left(1 + \frac{l_2}{l_1} - \frac{l_2}{f_2}\right)^2, \text{ at } \frac{l_1}{f_1} = \frac{a^X_{12}}{a^X_{11}} l_1 + \left(1 - \frac{l_2}{f_2}\right) / \left(1 - \frac{l_2}{f_2} + \frac{l_2}{l_1}\right) \quad (19)$$

and

$$\sigma^X_{11min} = a^X_{11} \left(\frac{l_2}{l_1}\right)^2, \text{ for any } \frac{1}{f_1}, \text{ when } \frac{l_2}{f_2} = 1 + \frac{l_2}{l_1} \quad (20)$$

The first solution shows the possibility to adjust the σ^X_{11} minimum by adjusting the gradient of the second magnet and thus lower the requirements for the resolution of the system. The second solution can not be used for the emittance calculation as it only gives information about the rms beam size $\sqrt{a^X_{11}}$ in front of the quadrupole magnet. It is possible to find the extremum for the Y direction as well. All solutions looks almost the same as (19) and (20), the only differences are the opposite signs of the quadrupole gradients. It is useful to consider the second solution for the Y direction:

$$\sigma^Y_{11} = a^Y_{11} \left(\frac{l_2}{l_1}\right)^2, \text{ for any } \frac{1}{f_1}, \text{ when } \frac{l_2}{f_2} = -1 - \frac{l_2}{l_1} \quad (21)$$

This is a very important result which allows to fix Y beam size at the radiator position. Moreover, this condition makes it easier to treat the data for the slice emittance measurements which use a streak readout where the signal in the Y direction is cut. After substitution $\frac{l_2}{f_2}$ from Eq. (21) in Eq. (19) the minimum σ^X_{11} becomes:

$$\sigma^X_{11min} = \frac{\varepsilon^2_{rms}}{a^X_{11}} 4 \left(l_1 + l_2\right)^2 \quad (22)$$

$\sqrt{\sigma^X_{11min}}$ is now 2 times higher than for the single quadrupole scan (Eq. (14)) when the setup length stays the same ($l = l_1 + l_2$). Thus, condition (21) fixes Y beam size which simplify the measurement procedure and increases $\sqrt{\sigma^X_{11min}}$ which lowers the requirements for the resolution of the measurement setup.

Eq. (22) gives guidelines for the optimization of the quadrupole scan setup. It is possible to increase $\sqrt{\sigma^X_{11min}}$ by enlarging a drift space $(l_1 + l_2)$. From the other side a total drift space of the setup should be small enough to reduce a space charge contribution to the measurements. In addition, beam size at the waist ($\sqrt{\sigma^X_{11min}}$) can be increased by focusing beam in X direction (decreasing a^X_{11}) in front of the first quadrupole. According to the Eq. (21) beam size in Y direction $\sqrt{\sigma^Y_{11}}$ can be tuned either by changing the ratio $\frac{l_2}{l_1}$ or changing Y beam size a^Y_{11} in front of the first quadrupole.

Although it could be interesting to consider a scheme with more than two quadrupoles, this report ends with the theoretical discussion only up to two quadrupoles. One of the reasons is the required drift spaces between the quadrupoles which elongate the measurement setup, and, therefore, the space charge effect contributes significantly to the measurements at the low beam momenta used at PITZ.

3 Experimental setup

Currently, a single quadrupole scan scheme is implemented in the high energy section at PITZ1.7 setup (Fig. 3) for the slice emittance measurements. Use of more than a single quadrupole is considered in Section 4. In order to characterize the electron bunch, the PITZ1.7 setup has numerous diagnostics in the low energy (downstream the gun) and high energy (downstream the booster) sections. The low energy dispersive arm is used to measure beam momentum downstream the gun and two high energy dispersive arms can be used to measure beam momentum downstream the booster. Bunch charge measurements can be done using faraday cups in the low energy section and by integrating current transformers in both the low and high energy sections. The current PITZ setup allows to achieve beam momenta up to 15 MeV/c after the booster. The quadrupole scan setup includes a quadrupole doublet, located at 5.19 m distance from the cathode and a screen station with a streak readout at a position of 6.345 m from the cathode. The distance between the quadrupoles is about 10 cm which is too small to use them for the double quadrupole scheme (Section 2.5). The effective length of the quadrupole is about 40 mm and the gradient can be varied from -7 T/m to +7 T/m. Calibration of the quadrupoles and the effective length measurements has to be done for each quadrupole separately (Appendix A). It is possible to estimate how good is the thin lens approximation for the PITZ setup using Eq. (5). The minimum focal length for a 15 MeV/c beam can be obtained at 7 T/m quadrupole gradient ($f = 180$ mm) which is still larger than the effective length of the quadrupole. Thus, all the conclusions from the theoretical section are valid for the current setup. There are more quadrupole doublets available downstream on the beam line although they are all installed after the screen station with a streak readout. Therefore one can use only a single quadrupole scan for slice emittance measurements at the moment and a multi-quadrupole scan can be used for projected emittance measurements.

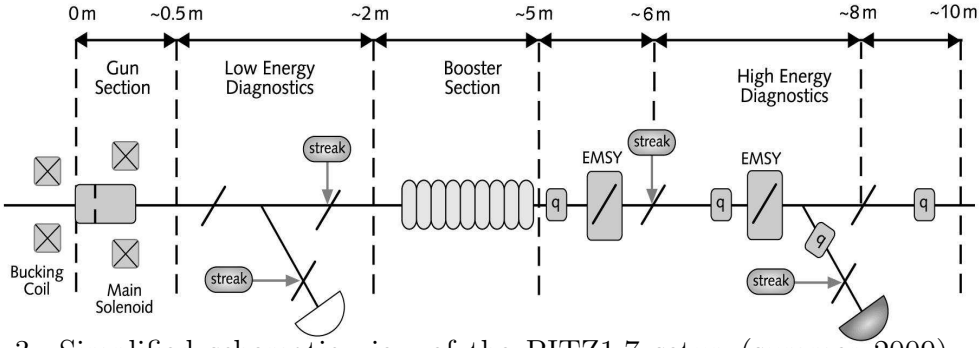

Figure 3: Simplified schematic view of the PITZ1.7 setup (summer 2009). The beam propagates from left to right.

A 5 mm thick aerogel [5] or OTR screen can be used for the time resolved measurements. Although an OTR radiator has much lower photon yield than an aerogel radiator [6] it has much better transverse resolution. Using properties of Cherenkov radiation [7], it is possible to estimate the point spread function for the aerogel radiator. The Cherenkov radiation angle for the current setup (15 MeV/c beam momentum and 1.008 index of refraction of aerogel) is 7 degrees. A schematic view of the Cherenkov process is shown in Fig. 4. A single electron will emit photons in the cone with an theta=7 degrees angle. Currently, the screen station at PITZ is equipped with an aerogel radiator which

can not be made thinner than 5 mm due to the production technology. After an electron passes through a L=5 mm thick radiator, it will produce an equally distributed light spot with a diameter d at the front surface of the radiator. Thus, the point spread function for the 5 mm thick source of the Cherenkov radiation will have a diameter:

$$d = 2 \cdot L \cdot tg(theta) = 2 \cdot 5\ mm \cdot tg(7^o) = 1.22\ mm \tag{23}$$

When the object plane is in the middle of the radiator then the point spread function diameter decreases to 0.61 mm which is the optimum case. This point spread function is far too large for obtaining good resolution. One can improve the resolution by introducing a partial cone scheme [6] but then the light collection reduces significantly. For this reason an OTR screen is preferable. A 30 m long optical line is used to transport light from the radiator to the streak camera [8]. The current optical system includes about 12 lenses. If the broad spectrum of the OTR radiation is used, dispersion in the optical system limits the temporal resolution to about 70 ps. Therefore, a 10 nm bandwidth filter has to be applied to measure the longitudinal distribution with about 3 ps resolution. The drawback of the filter is a big reduction in the signal intensity as OTR and aerogel radiators have a broad light spectrum. The spatial resolution of the optical beam line was measured to be 15 line pairs/mm [6].

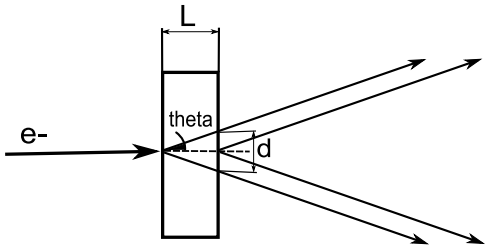

Figure 4: Schematic view of the Cherenkov radiation process.

A slit is used in front of the streak camera for the time resolved measurements. The slit width can be varied from 0 to several millimeters. A nominal width of 100 μm is usually used for the measurements. The height of the slit is about 5.4 mm. Since the slit introduces a strong asymmetry to the image it would be useful to have asymmetric focussing before the slit entrance. Cylindrical lens can be considered for such a focussing as they are focussing only in one direction. However, a cylindrical lens will worsen the transverse resolution and complicates the optical system. Imaging from the slit to the photocathode was done by reflective optics. After the rotation of the time axes in the streak unit to one of the transverse axes, electrons are converted back to photons and are then imaged on to a CCD camera. The longitudinal resolution of the streak camera depends on the slit width and is about 2.5 ps for a 100 μm slit. The total longitudinal resolution of the system is estimated as 4 ps. The overall current optical system magnification is equal to 0.5.

The current PITZ1.7 setup will be upgraded to PITZ2.0 (Fig. 5). The major upgrade is planned for Autumn 2009. It includes installation of a new booster cavity and the phase space tomography section with about 9 quadrupoles. The new booster cavity will be able to accelerate electron bunches up to 30 MeV/c momentum. The additional

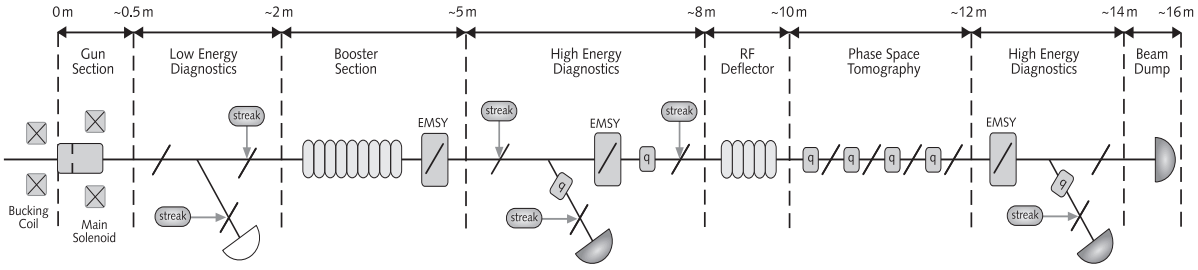

Figure 5: Simplified schematic view of the PITZ2.0 setup (includes future upgrades). The beam propagates from left to right.

variety of quadrupoles in the PITZ2.0 setup gives the possibility to optimize a multi-quadrupole scan system for emittance measurements. Unfortunately neither of the screen stations in the tomography module in the first installation will have streak readout. After the optimization of the quadrupoles and screen positions, the streak readout has to be designed for the corresponding screen station. Using Eq. (21) it is possible to obtain the main restriction for the setup geometry:

$$\frac{1}{l_1} + \frac{1}{l_2} = \frac{1}{|f_2|} < \frac{1}{|f_2^{min}|} \tag{24}$$

Suppose that $l_1 = l_2$, the beam momentum is 30 MeV/c and the maximum possible quadrupole gradient is 7 T/m. After substituting (4) and (5) in (24), the restriction becomes:

$$l_1 = l_2 > 2 \cdot \frac{p[Gev/c]}{0.2998 \cdot g[T/m] \cdot lef[m]} = 0.71\ m \tag{25}$$

One example of the multi-quadrupole scan in the tomography section is shown in Section 4.5.

4 Simulation results

4.1 Simulation routine

The main topic of this section is a quadrupole scan experiment simulation and estimation of possible systematic errors. ASTRA [9] scientific software was used to track the electron beam to the screen position, including a space charge routine. Afterwards, the output beam distribution was convoluted with a gauss point spread function:

$$g(x) = \frac{1}{\sigma\sqrt{2\pi}} e^{-\frac{x^2}{2\sigma^2}} \tag{26}$$

in order to take into account the finite optical resolution. The rms size of the point spread function (σ) was taken to be 100 μm which approximately corresponds to the setup performance. Fig. 6 shows the result of the convolution procedure. It is clear that after the convolution the rms size of the distribution increases and all details within a 100 μm range are smeared out. Finally, the obtained distribution was cut with a 100 μm

slit width. An example of the slit cut is shown in Fig. 7. The red lines indicate the slit location: only signal between these lines can pass through the slit. The major part of the signal distribution in this example is dumped on a slit. Furthermore, the central part of the beam distribution has higher beam size which causes additional systematic error. Thus, three main types of systematic errors were taken into account: space charge forces, finite optical resolution and the cutting of the signal with a slit. Although, the thin lens approximation could be used, matrices from Eq. (3) were used for Eq. (8) to fit the data and obtain the emittance values. The resultant emittance was compared to that given by the ASTRA output in front of the quadrupole. Simulations were performed for the current PITZ setup (PITZ-1.7 with a maximum beam momentum 15 MeV/c) and for the future setup (PITZ-2.0 with a nominal beam momentum 30 MeV/c).

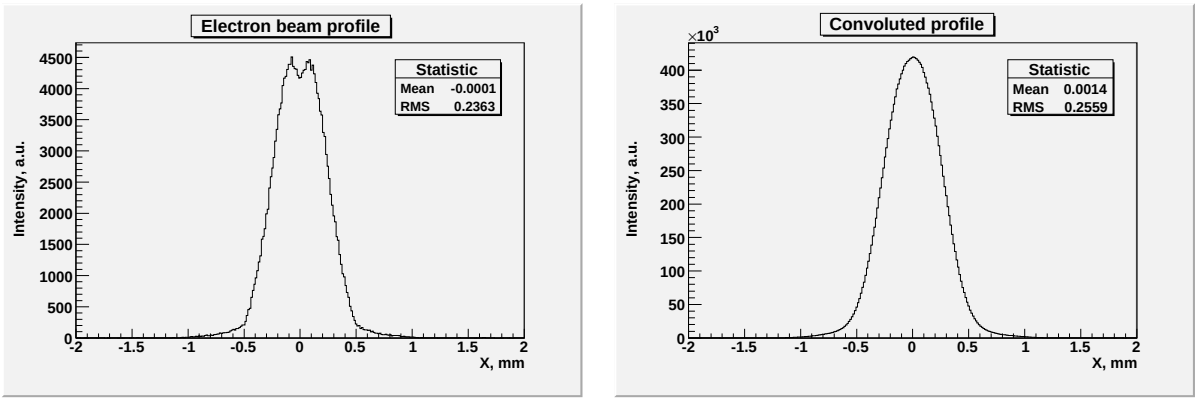

Figure 6: Simulated example of the convolution procedure. ASTRA output of an electron beam distribution at the screen position (left) and convolution of this distribution with a gaussian point spread function (right).

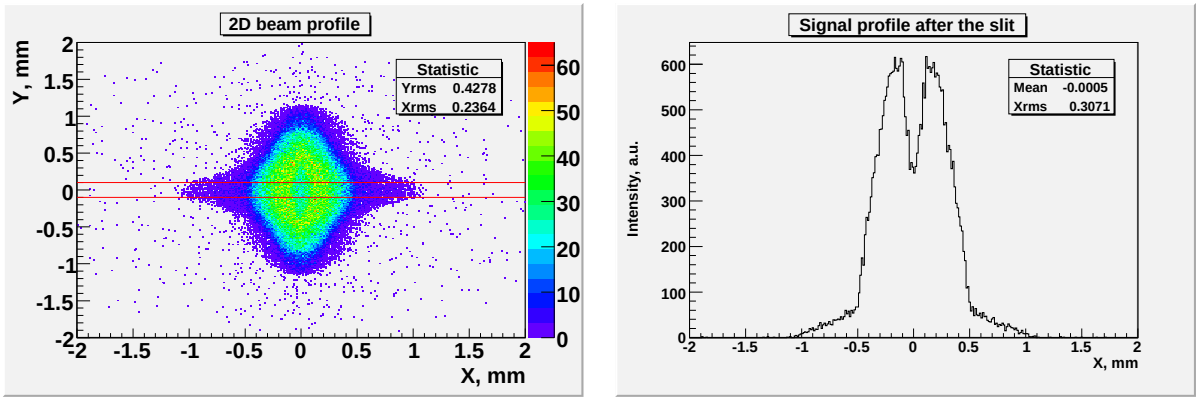

Figure 7: Simulated example of the signal cut with a slit. Initial 2D signal distribution together with a slit view (left) and 1D signal profile after the slit (part of the signal between the red lines).

4.2 Beam dynamics before the quadrupole entrance

In order to simulate quadrupole scan experiment, first of all it is necessary to obtain the electron beam distribution which is expected in the measurements. For this purpose emittance optimization at High1.Q1 entrance (5.13 meters from the cathode) was performed. The longitudinal laser shape for the current simulations was a flat top with a 20 ps full width at half maximum(FWHM) and 2 ps rise and fall times [10]. The transverse profile of the laser was a circular flat top with 0.47 mm rms size in both directions. 1 nC bunch charge was extracted from the photocathode. The laser transverse size was optimized simultaneously with the solenoid field. The gun and the booster gradients were tuned to get maximum mean momentum gain resulting in 6.68 MeV/m after the gun and 14.44 MeV/c (30 MeV/c) after the booster which correspond to the typical experimental conditions. Gun and booster phases were set to the phase of maximum mean momentum gain as they do not have a major influence on the emittance. ASTRA 2D space charge routine was used to track electrons from the cathode to the entrance of High1.Q1.

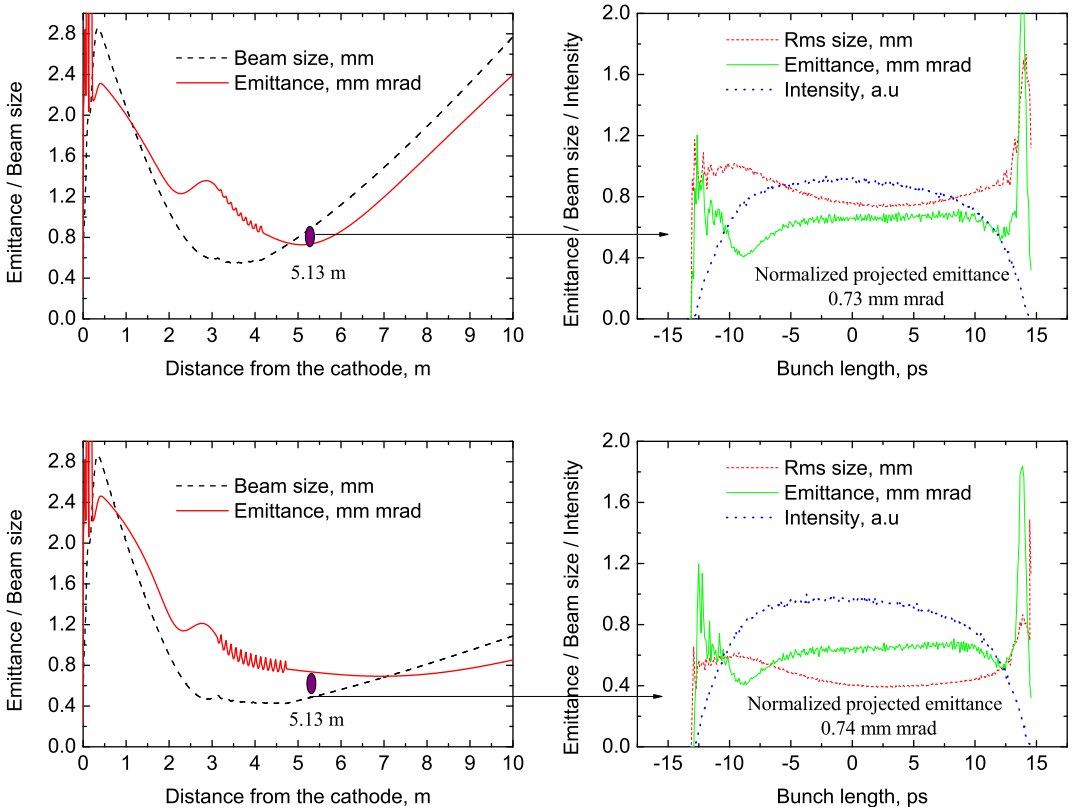

Figure 8: Beam dynamics simulation for PITZ-1.7 setup with a beam momentum of 14.44 MeV/c (top) and PTIZ2.0 setup with a beam momentum of 30 MeV/c (bottom). The left graphs show the beam size and emittance versus distance from the cathode. The right graphs describe the longitudinal properties of the electron bunch 5.13 meters downstream the cathode (Hiqh1.Q1 entrance). The solenoid current and transverse laser beam size were optimized in order to get minimum emittance at the Hiqh1.Q1 entrance.

Figure 8 shows the evolution of the emittance and the beam size versus the distance

from the cathode (left) and longitudinal beam properties at the entrance of the High1.Q1 (right). The minimum normalized projected emittance of 0.73-0.74 mm mrad was obtained at the entrance of the High1.Q1 during the optimization. Although the middle part of the bunch has almost constant emittance at the level of 0.65 mm mrad, the finite rise and fall time of the laser pulse increases the emittance of the head and tail. Thus, the head and the tail of the bunch contribute to the projected emittance growth. There is almost no difference in the projected and the slice emittances for the optimum point for 14.44 MeV/c and 30 MeV/c beam momenta. However, the emittance of the 30 MeV/c beam does not grow as fast as for the 14.44 MeV/c case during the propagation. Although, the higher momentum beam has less space charge influence and an emittance change over the long drift space, it is clear that doubling the beam momentum halves the beam size at the minimum location (see Eq. (14)). This would be a critical point for decision on whether to use the higher momentum beam for the measurements. Luckily, this effect is compensated by the decreased beam size at the quadrupole entrance (Fig. 8). Thus, the minimum beam size at the observation screen during the quadrupole scan will be approximately the same for both beam momenta cases, 14.44 MeV/c and 30 MeV/c. Taking into account the longitudinal resolution of the setup, the longitudinal properties of the bunch are always calculated for 4 ps slices (Fig. 9). The head and tail of the bunch have higher emittance values than the middle part. Therefore, all estimations of the systematic errors, obtained in the next sections, are averaged over 5 middle slices.

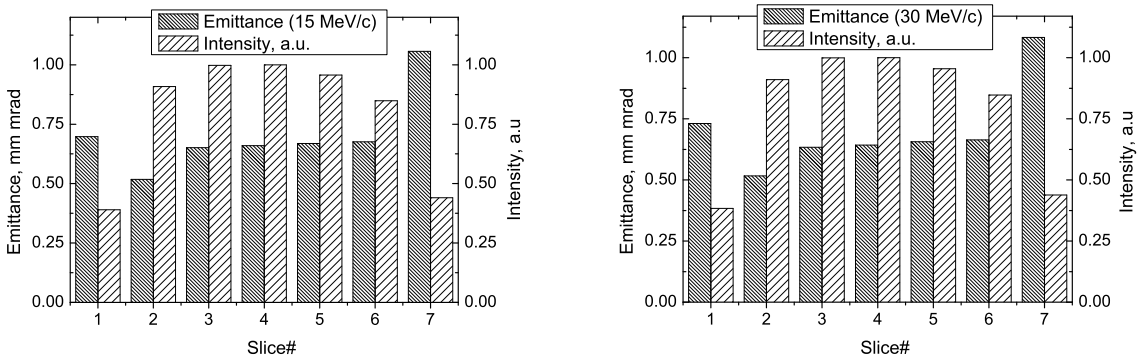

Figure 9: Slice emittance of 14.44 MeV/c (left) and 30 MeV/c (right) beams in front of the quadrupole. Each slice has 4 ps length.

4.3 Single quadrupole scan

Using an expected beam size (0.8 mm) and emittance (0.65 mm mrad) of the middle slice (14.44 MeV/c case) in front of the quadrupole and a known drift space (l=1.115 m), it is easy to estimate a minimum beam size which has to be measured (Eq. (14)): $\sqrt{\sigma_{11min}} = 32\ \mu m$. This value is three times lower than the size of the point spread function, which will result in about three times increase of the measured emittance in comparison to the real one [11]. Complex measurement simulation was performed to determine the contribution to the systematic error for each source: space charge, finite optical resolution and a 100 μm slit width (see Section 4.1). The ASTRA 3D space charge routine

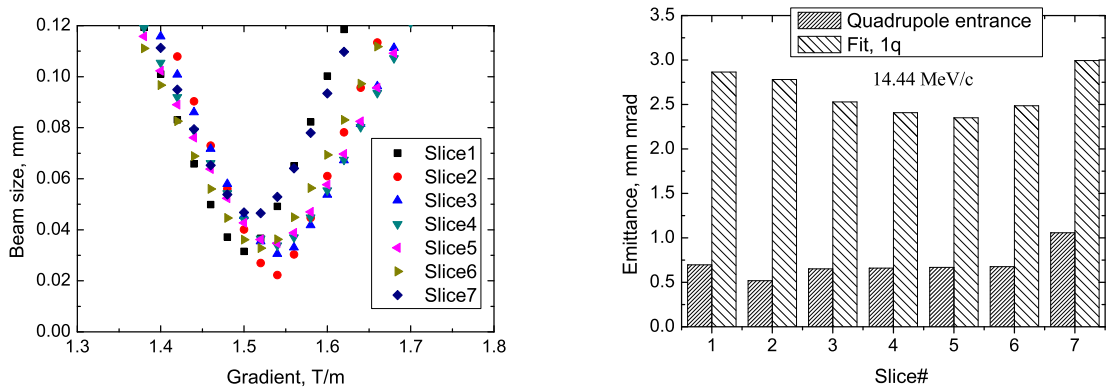

Figure 10: Expected beam size at the screen location (left) and emittance measurement results (right) for a single quadrupole scan at a 14.44 MeV/c beam momentum.

was used to track the particle distribution from the quadrupole entrance to the screen position. Fig. 10 shows expected results from the single quadrupole scan measurements. The average error for the five middle slices is about +300 %. The partial contributions to the systematic error in the measurements averaged over the five middle slices are shown in Table 1. As expected, the main contribution comes from the low optical resolution for such small beam sizes. Although Table 1 shows an error of each individual contribution, partial errors are dependent on the contributions listed in the previous line because all errors were calculated in sequence. For example, if there is only a contribution from the 100 μm slit width, the systematic error in the measurements would be 35 % instead of 62 %. The other important issue is a large beam size in the Y direction (perpendicular to the measurement). Thus, only a small part of the signal could pass through a 100 μm slit width, which means a low intense signal at the streak camera and that the measurements include only information about a small part of the distribution. Moveover, the amount of signal depends on the quadrupole current. Simulations show that only about 2.6 % of the total charge passes through the 100 μm slit width. Although the simulations above were performed for the 14.44 MeV/c beam momentum, similar results can be obtained for 30 MeV/c beam momentum.

Table 1: Error contributions to the slice emittance measurements for a single quadrupole scan. All errors are averaged over five middle slices.

Error source	Error, %	Contribution, %
Space charge	+3	1
100 μm optical resolution	+237	78
100 μm slit width	+62	21
Total	302 %	100 %

A possible improvement of the single quadrupole setup could be to increase the drift space in order to reduce the effect of the optical resolution limit. On the other hand, this solution results in an even more spread beam distribution in Y direction which decreases

the amount of signal coming through the slit. Furthermore, increase of the drift space leads to the larger space charge contribution to the systematic error.

4.4 Double quadrupole scan

It was already shown that a single quadrupole scan delivers very tiny beam sizes at the screen which cannot be resolved. The other disadvantage of the single quadrupole scan is a big variety of the beam sizes in the direction perpendicular to the measurement direction depending on the quadrupole gradient. This leads to a different amount of signal coming through the streak camera slit for the different quadrupole gradients. A double quadrupole scan can be used in order to improve both disadvantages of the single-quadrupole scan. Accordingly to the theoretical prediction of Section 2, it is possible to lower requirements on the resolution of our optical system and keep a constant beam size in the non-measurement direction already with two quadrupoles.

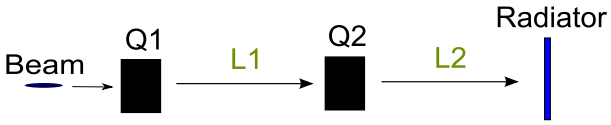

Figure 11: Double quadrupole scan scheme.

The ASTRA 3D space charge routine was used to propagate the electron bunch distribution from the first quadrupole entrance to the screen location. The double quadrupole scheme is shown in Fig. 11 where Q1 is the first quadrupole which corresponds to High1.Q1 (5.19 meters from the cathode in PITZ-1.7 and PITZ-2.0 schemes), Q2 corresponds to High1.Q3 (6.83 meters from the cathode), L1 is the drift space between the first and the second quadrupoles, L2 is a drift space from the second quadrupole to the radiator (screen). Three screen locations were used for the simulations: EMSY2 (7.125 m from the cathode), High1.Scr4 (8.387 m) and High1.Scr5 (8.982 m). These simulations were done just to understand the behavior of each systematic error type as neither of those screens have a streak readout. However, the measurement of the projected emittance would be possible using any of these screens.

Table 2: Screen locations as a distance from the cathode and corresponding gradients of the second quadrupole for the double quadrupole scan.

Screen name	Screen location	High1.Q3 (14.44 MeV/c)	High1.Q3 (30 MeV/c)
EMSY2	7.125 m	4.36 T/m	8.96 T/m
High1.Scr4	8.387 m	1.56 T/m	3.2 T/m
High1.Scr5	8.982 m	1.36 T/m	2.78 T/m

According to the theoretical description (Section 2), the second quadrupole current should be constant and it depends only on the setup geometry and the beam momentum. Experiment simulations were performed for both 14.44 MeV/c and 30 MeV/c beam momenta. Table 2 shows the screen locations and necessary High1.Q2 gradients to fulfill

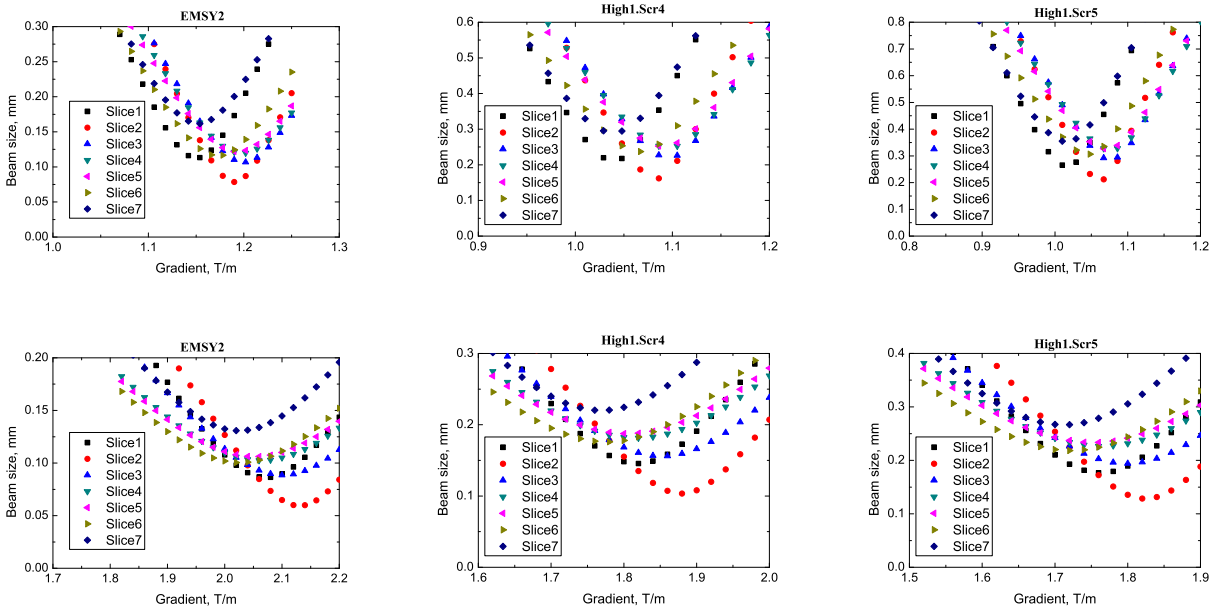

Figure 12: Expected beam size at three different screen locations for a double quadrupole scan with a 14.44 MeV/c beam momentum (top row) and 30 MeV/c beam momentum (bottom row).

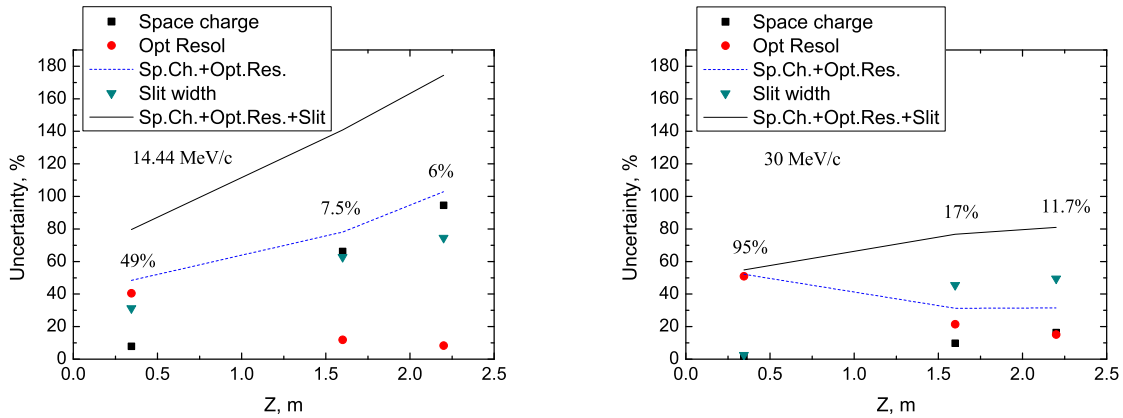

Figure 13: Emittance systematic error of the double quadrupole scan measurements for the three screen locations and for 14.44 MeV/c (left) and 30 MeV/c (right) beam momentums. Z=0 corresponds to the position of the second quadrupole, Hiqh1.Q3. All numbers are average values over the 5 middle slices. Percentage of the signal which is coming through the 100 $m\mu$ slit width is shown on top of each point.

condition (21). It is clear that the case of EMSY2 observation screen and a 30 MeV/c beam momentum can not be realized in practise due to the required high quadrupole gradient, however it is useful to simulate this case. To estimate the systematic error for each case, the same procedure was repeated as in Section 4.3. Figure 12 shows beam size dependence versus quadrupole gradient for different screen locations and beam momenta. As

a result of the simulations the expected systematic error in the emittance measurements is shown in Fig. 13. Three different contributions to the error were considered: space charge effects, finite optical resolution (100 μm rms of the point spread function) and a slit in front of the streak camera (100 μm slit width). The contribution of space charge effects is growing with drift space and is high for the low energetic case. As predicted by Eq. (22) the beam size at the waist is increasing with a drift space and optical resolution limitation gives less error when the drift space is elongated. The Sp.Ch.+Opt.Res. line summarizes the contributions from the space charge and finite optical resolution. If PITZ would have a gaussian transverse beam distribution, cutting the beam with a slit would not contribute to the error. In reality, the PITZ injector has far from a gaussian transverse beam profile. Moreover, the central part of the beam has higher beam size during the quadrupole scan which increases the measured emittance when the beam is cut with a slit (Fig. 13). The overall error for a 30 MeV/c case is smaller than for a 14.44 MeV/c.

The Sp.Ch.+Opt.Res.+Slit line includes all three types of error considered. Theoretically it is possible to make a beam profile scan over the Y direction for each quadrupole current. Thus, the total error (Sp.Ch.+Opt.Res.+Slit) will be decreased to the contribution of the space charge and optical resolution (Sp.Ch.+Opt.Res.). However, such an action does not improve the signal to noise ratio and complicates the measurement procedure and it would be better just to increase the amount of signal passing through the slit and therefore decrease the error contribution from the slit width. The overall error (Sp.Ch.+Opt.Res.+Slit) is still too high for all cases. Thus, one should make an optimization with focusing the beam in front of the scanning quadrupole.

4.5 Use of four quadrupoles

Additional improvement in the error can be achieved when the beam is focused in front of the quadrupole (Eqs. (22) (21)). Two additional quadrupoles must be used for this purpose (Fig. 14). The distance between the quadrupoles Q1 and Q2 must be small enough to have symmetric conditions for the focussing in X and Y directions.

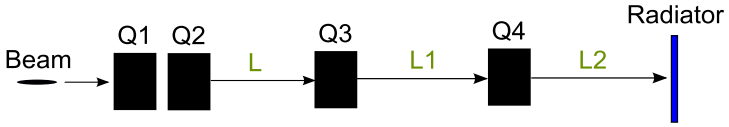

Figure 14: Four quadrupole scheme. Q1 and Q2 are used to focus the beam in front of the scanning quadrupole Q3.

The drift space between Q3 and the radiator must be below 2 meters in order to decrease the space charge contribution. As an example, the setup geometry was chosen in agreement with the PITZ-2.0 setup:

Element	Name	Location
Q1	High1.Q5	10.208 m
Q2	High1.Q6	10.388 m
Q3	PST.QM1	12.088 m
Q4	PST.QM3	12.848 m
Radiator	PST.Scr3	13.789 m

All distances are shown with respect to the cathode location. Quadrupole scan simulations were performed using the geometry described above together with an input beam distribution described in Section 4.2 for 30 MeV/c beam momentum. Q1 and Q2 gradients were set to -5.4 T/m and 5.6 T/m, respectively, in order to obtain a good focussing. The resulting beam dimensions in front of Q3 are focussed to 0.13 mm rms size in X direction and 0.07 mm in Y direction. The gradient of Q4 was constant and set to -6.13 T/m, according to the condition (21). Under this condition 79% of the signal is passing through the 100 μm slit. Theoretically it would be better to decrease the ratio L2/L1 and therefore to relax the focussing in the Y direction but it is necessary to find a compromise between the existing setup and the optimum conditions.

Table 3: Error contributions to the slice emittance measurements for a double quadrupole scan using additional focusing. 30 MeV/c beam momentum. All errors are averaged over the five middle slices.

Error source	Error, %	Contribution, %
Space charge	+1.3	12
100 μm optical resolution	+6.5	63
100 μm slit width	+2.6	25
Total	10.4 %	100 %

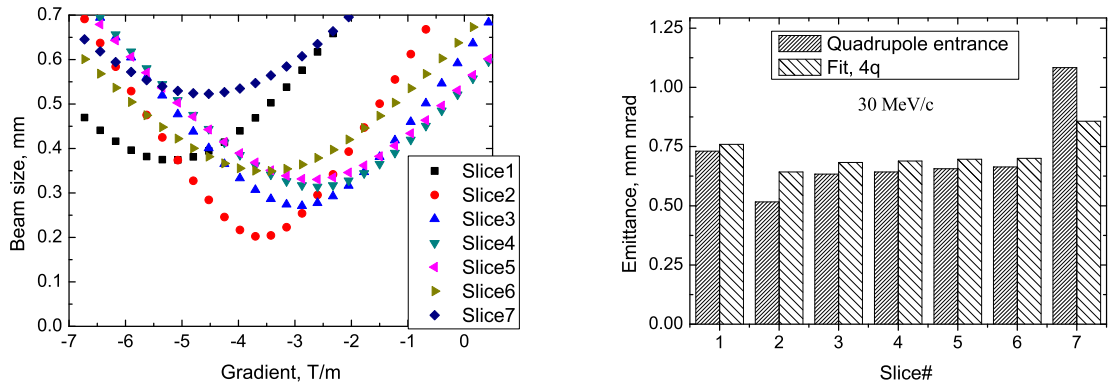

Figure 15: Expected beam size at the screen location (left) and expectation of the slice emittance measurement results (right) of a 30 MeV/c beam. All slices have 4 ps length.

An expected beam size at the screen location is shown in Fig. 15 (left) as a function of Q3 gradient. The fitted result of the simulated experiment is shown in Fig. 15 (right). It is already clear that the resolution of such a scheme is good enough to measure the required slice emittance. All contributions to the systematic error for the five middle slices are summarized in Table 3. The total error is in the order of 10%. Q1 and Q2 gradients can be tuned for the error optimization if either the setup geometry or setup performance is changed. All slices have positive systematic error except the head of the bunch (slice number 7). The head of the bunch has lower measured emittance than the original one (see Fig. 15 (right)) due to the reduction of the beam size after applying a 100 μm slit width. This effect most probably appears due to insufficient particle statistics for the halo part of the last slice as the transverse dimensions of the last slice are already fairly large (see Fig. 15 (left))).

5 Projected emittance measurements

Presently, there is no streak readout available after the High1.Q3 quadrupole. Therefore, the methodical measurements of the projected emittance were performed using the double quadrupole scheme (Fig. 11). It is useful to mention that the performance of the projected emittance measurement using a quadrupole scan method is quite different from the slice emittance measurement. Firstly, there is no error due to the beam cut as there is no slit to be applied and the beam size is limited only by the screen size. Secondly, the resolution of the optical system is much better than 100 μm. Thus, the only importance is the space charge contribution which is always growing with an increasing drift space. Taking this into account, the measurements were performed using EMSY2 as an observation screen. The setup geometry is exactly the same as it was described in Section 4.4. The quadrupole scan measurements followed immediately after the slit scan measurements of the projected emittance. The main parameters during the measurements are summarized in Table 4.

Table 4: Main machine and beam parameters during the quadrupole scan measurements. Zero cavity phase corresponds to the phase of maximum mean momentum gain. Negative cavity phase is going to the direction of the larger momentum spread.

Laser:	Xrms, mm	Yrms, mm	FWHM, ps	rise, ps	fall, ps
	0.43	0.44	23.05	2.23	1.96
Beam momentum, Mev/c	after the gun		after the booster		
	6.65		14.48		
Phase, degree	Gun phase		Booster phase		
	-8		0		
Bunch charge, nC	1.0				

The current of High1.Q3 was constant and set to +/-5.85 A which should correspond to +/-4.261 T/m, as required by condition (21). A positive sign was applied for the X emittance measurements and a negative sign was applied for the Y emittance measurements. Emittance was measured for several solenoid currents for X and Y projections (Fig. 16). One can see that the value of the emittance is much higher than the optimized theoretical prediction (Section 4.2).

After the measurements reported in this paper have been performed it was found that the current PITZ setup had some magnetized components in the beam line which caused a coupling between X and Y phase spaces of the electron beam. It means that our first assumption of no XY correlation was wrong. Meanwhile those magnetized components were removed. Moreover the conditions for the quadrupole scan were not fully optimized during the measurements. It would be necessary to have a more detailed solenoid scan as well as optimized gun and booster phases. It is possible that the beam momentum spread contributes to the systematic error when gun phase is set off-crest to -8 degrees due to the additional slices rotation when applying quadrupoles. In general, the gun phase should be adjusted to minimize the beam momentum spread. The quadrupole scan measurement results for a solenoid current of 382 A are shown in Fig. 17. The beam size in the non-measurement direction is almost constant with small deviations which could be due to the space charge effect. Another important feature of the measurements is that the beam

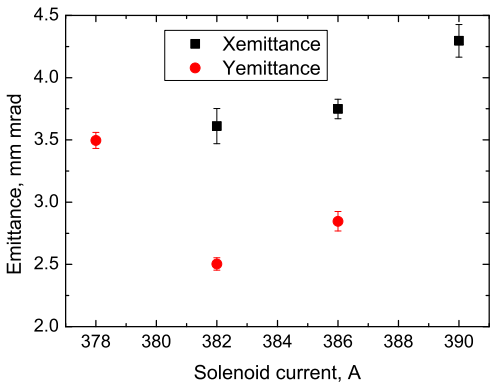

Figure 16: Emittance measurement results versus solenoid current using a double quadrupole scan.

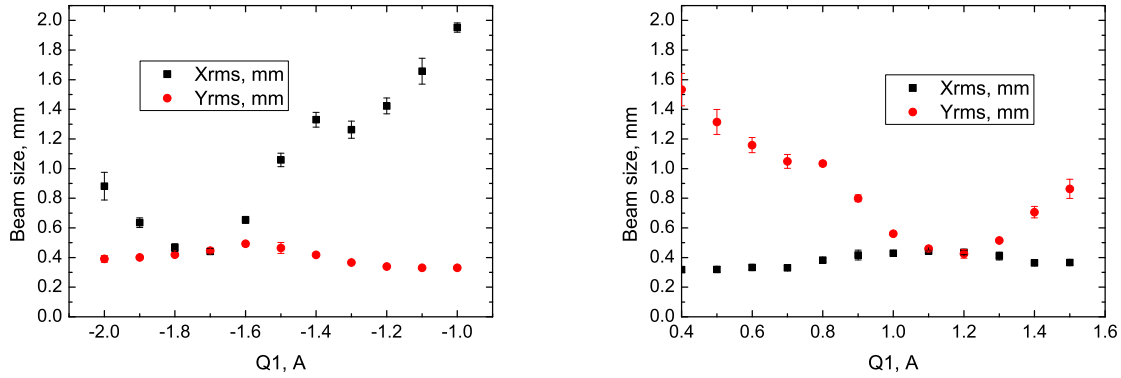

Figure 17: Quadrupole scan measurements of X emittance (left) and Y emittance (right) at Imain = 382A.

size does not show a smooth dependance on quadrupole current but has a displacement at some quadrupole currents for both X and Y emittance measurements. More detailed investigations show the influence of the beam halo contribution to the measurements when focussing with the quadrupoles (see Fig. 18), which can not be seen for the non-focussed beam because of its low intensity. It was found that this halo was produced by a non-perfect laser shape on the photocathode and it contributes significantly to the beam size measurements which raises the values of the measured emittance. An additional problem arises due to the high signal intensity when the beam is focussed. It starts to saturate the camera which is unavoidable even if the camera gain is decreased to the lowest possible value and a single laser pulse is used.

Figure 18 shows a comparison of the measured profiles with the simulated profiles during the double quadrupole scan for the same operation conditions. The measured and simulated beam profiles have similar structures. However, the dimensions of the measured beam are visibly higher than the simulated one. Also there is a beam halo (Fig. 18 top-

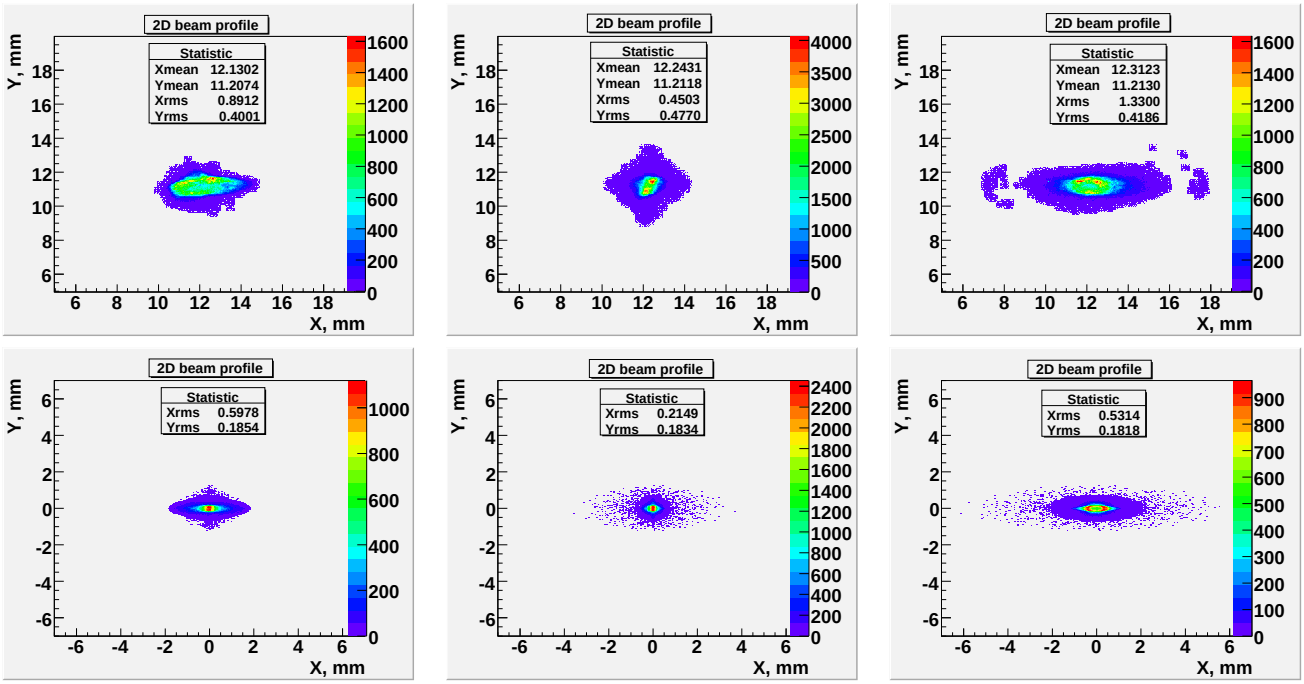

Figure 18: 2D beam profiles during the double quadrupole scan experiment for the projected X emittance measurement (top row) and simulations (bottom row). Beam profiles at approximately -0.15 T/m from the horizontal focus (left column, over focused beam), in the horizontal focus (middle) and at +0.15 T/m from the horizontal focus (right column, under focused beam).

right) which is not predicted by the simulation results. It is useful to notice that the over focused beam (Fig. 18 left) is not fully symmetric and has a very different profile compared to the simulated one.

6 Summary

Knowledge of the slice emittance plays an important role in the optimization of high brightness electron sources for short wavelength FELs. For RF photoelectron guns there is a strong space charge influence during the photoemission and early stage acceleration. Space charge has a different effect on the different longitudinal slices of the electron beam which is not possible to determine from projected emittance measurements. Therefore, it is important to know the emittance distribution within the electron bunch (slice emittance). Time resolved emittance measurements can be done by aerogel or OTR radiators with streak camera readout at PITZ. According to the measurement setup, the resulting transverse resolution of the aerogel radiator is not sufficient and OTR screens have to be used. A 30 meters long optical transmission line is used to transport the light from the radiator to the streak camera. This system contains approximately 12 lenses and has strong dispersion and poor transverse resolution (100 μm). A 10 nm bandwidth filter has to be used to reduce the effect of dispersion and the complete streak system has a total time resolution of about 4 ps. The currently available PITZ setup with a single quadrupole scan has insufficient transverse resolution to measure slice emittances down to 0.6 mm mrad.

Therefore, a multiquadrupole scan technique for slice emittance measurements has been developed using up to four quadrupoles. This technique lowers the requirements on the setup resolution and offers more possibilities to control the beam dimensions during measurements. Already, a two quadrupole scheme can have a total systematic error of about 50% for 30 MeV/c beam momentum. Moreover, the use of four quadrupoles lowers the systematic error to below 20%. Thus, exploiting the advantages of the multiquadrupole scan scheme, it is possible to lower the resolution requirements far enough to obtain reasonable slice emittance measurements with current streak optics. Furthermore, this technique will improve the situation with low signal intensity as for the current setup with a single quadrupole scan only about 3% of the signal can pass through the slit in front of the streak camera. The four quadrupole scheme allows more than 90% of the signal to pass through the 100μm slit width. As expected, simulations predict improved performance of the setup when using a higher electron beam momentum.

The experimental measurement procedure was tested for projected emittance measurements using a double quadrupole scan scheme. However, the optimization of the machine parameters (main solenoid current, gun and booster phases) should be carried out more precisely to achieve reliable projected emittance measurement results. Saturation of the camera should be avoided by either decreasing the aperture of the screen optics or using an OTR screen which has less light yield than the YAG screen, which is currently used.

The next important step would be to optimize the location of the setup components for the slice emittance measurements using a four quadrupole scan according to the existing quadrupole and screen positions in the tomography section. After this optimization one of the tomography screen station can be redesigned and equipped with a streak readout.

The projected emittance measurements should be performed by the tomography reconstruction, slit scan and multiquadrupole scan methods for the same conditions in order to compare these techniques. The comparison would be especially interesting for the high momentum case when emittance does not change significantly during the beam propagation along the beam line.

It is useful to study the influence of the momentum spread of the beam on the projected and slice emittance measurements with a quadrupole scan technique. Therefore, the emittance measurements simulation should be performed for the different gun and booster phases. In addition, it would be useful to simulate multiquadrupole scan experiments for the different charges of the bunch.

7 Acknowledgments

First of all I would like to thank Dr. U.Gensch and Prof. J.Rossbach for the opportunity to work at one of the modern accelerator facilities. Also I am thankful to all the PITZ group for their valuable support and discussions during my work at DESY, especially to Dr. Frank Stephan, Dr. Mikhail Krasilnikov and Dr. Jürgen Bähr for their impact on my work.

A Appendix: Calibration of the quadrupoles

Calibration of the quadrupole magnets influences on the uncertainty of the emittance measurements using quadrupole scan technique. Quadrupoles used during the experiment were produced and calibrated by DANFYSIK company. The calibration was done with a maximum driving current of 12 A. Each quadrupole magnet was trained by applying currents from 0 A to 12 A several times before the data was taken. The last data set from 0 A to 12 A (bottom curve) and then from 12 A back to 0 A (top curve) was recorded (Fig. 19). Calibration results show good linearity up to about 9 A. Driving a quadrupole current to the maximum value +12 A and then using the calibration curve taken from 12 A back to 0 A (top curve) it is possible to reproduce quadrupole gradient up to 0.02 T/m. However, the maximum allowed range of the currents was restricted from -10 A to +10 A during the operation. The calibration data was interpolated with a 4th order polynomial with an interpolation range up to 10 A as it was the maximum possible value. Experimental data (Section 5) was fitted using both curves on the calibration graphs and the averaged emittance value is presented. Due to the uncertainty in the quadrupole calibration, there is an additional systematic error in emittance measurement which was estimated to be ±10%.

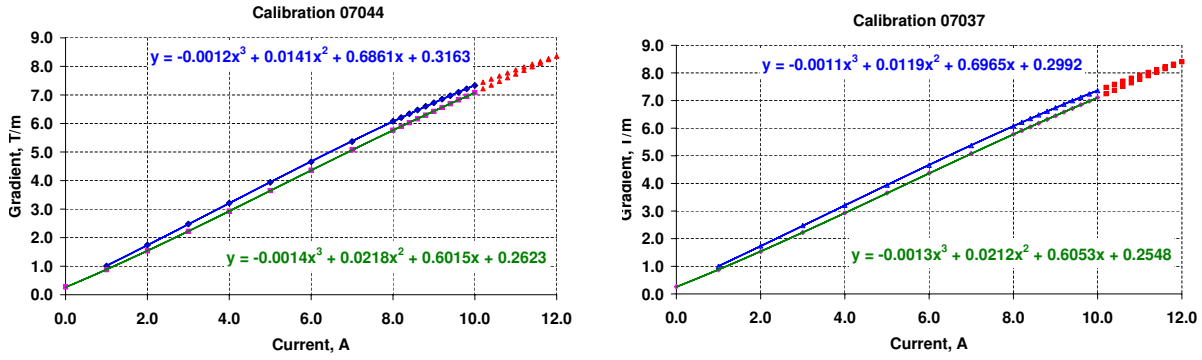

Figure 19: Calibration of the quadrupole magnets N07044 (left), located at High1.Q1 position and N07037 (right), located at High1.Q3 position. Quadrupoles were calibrated by DANFYSIK.

Designed effective length of this quadrupole type is 40 mm. However, the real effective length has to be measured for each quadrupole separately after the production. These measurements were performed by DANFYSIK company. The results of the measurements are summarized in Table 5.

Table 5: Results of the effective length measurements.

Quadrupole N	PITZ name	Effective length
07044	High1.Q1	42.9 mm
07037	High1.Q3	42.9 mm

References

[1] Helmut Wiedemann, Particle Accelerator Physics, Part II Beam Dynamics, Berliner Springer, Berlin, 3rd edition, (2007).

[2] Christopheer K. Allen and Nicholas D. Prattengale, Theory and Technique of Beam Envelope Simulation, Los Alamos Natioanl Laboratory, Los Alamos, (2002).

[3] J. Rossbach, P. Schmüsser, Basic Course on Accelerator Optics CAS - CERN Accelerator School, (1993).

[4] Frank J. Sacherer, RMS Envelope Equations with Space Charge CERN internal report, SI/Int. DL/70-12, (1970).

[5] J. Bähr, V. Djordjadze, D. Lipka, A. Onuchin, F. Stephan Silica aerogel radiators for bunch length measurements, Nucl. Instr. and Meth. A538, 597 (2005).

[6] J. Bähr, H.Luedecke, J.Roensch, Optical System for Measuring Electron Bunch Length and Longitudinal Phase Space at PITZ: Extension and Methodical Investigations, Proceedings of DIPAC, Venice, Italy, (2007).

[7] Claus Grupen, Cambridge Monographs on Particle Physics, Nuclear Physics and Cosmology, vol. 5, Particle Detectors, chapter 6, pp. 193-200 Cambridge University Press, (1996).

[8] J. Bähr, D. Lipka, H. Luedecke, Optical Transmission Line For Streak Camera Measurements at PITZ, Proceedings of DIPAC, Mainz, Germany, (2003).

[9] K. Floetmann, A Space Charge Tracking Algorithm (ASTRA), `http://www.desy.de/~mpyflo/`, updated February (2009).

[10] Ingo Will and Guido Klemz, Generation of flat-top picosecond pulses by coherent pulse stacking in a multicrystal birefringent filter, Opt. Express 16, 14922-14937 (2008).

[11] R. Spesyvtsev, et al., A transverse slice emittance measurement system using quadrupole scan technique and streak readout at PITZ, in Proceedings of the FEL 2008, Gyeongju, S. Korea, August (2008).